Analyzing the Effect of Soft Arm Design on Obstacle Navigation through Collision

Abigail Rafter[1], Geoffrey A. Hollinger[2], Yiğit Mengüç[2,3], and Gina Olson[2]

Abstract— The study of soft robot arms is often motivated by safe operation in contact or collision, such as an arm reaching into a tube, squeezing under a barrier or wrapping around an object. Existing work focuses on soft grasping, while collision-allowed navigation is neglected. Soft arms are not guaranteed to successfully push past obstacles simply because the arms are soft, but design rules for arms in collision have not been developed. This paper presents an initial empirical examination of planar arms in collision and specifically studies the relationship between key arm design variables – length, number of segments, taper – and the arm's ability to push past a semi-circular obstacle. Fourteen variants of a planar arm design were built and tested to determine the pressure required to push past the obstacle at a set of known locations. The pressure required was measured for actuation of one and multiple segments. The results were used to develop an empirical collision success model, which can be used with collision-allowed planning algorithms. Soft arms that balance flexibility, or range of motion, and applied force successfully push past obstacles in the largest range of locations. Flexibility and force are opposing traits driven by arm width; wider arm segments produce more force but have a smaller angular stroke and are harder to passively bend. This work serves as a foundation for future studies with a broader set of obstacle types and locations, which could be used to develop a robust collision model.

I. INTRODUCTION

Soft robots seek to mimic the flexibility and variable stiffness of cephalopod arms in order to perform tasks that traditional robots cannot complete safely. These robots are proposed for applications that require handling delicate or oddly shaped objects [1], conforming to or around unknown barriers in the environment [2] and moving through cluttered environments [3]. Traditional robots have speed and strength but lack the flexibility and delicacy that soft robots strive for, which allows soft robots to interact safely and smoothly with their environments. A traditional robot arm operating in a cluttered environment must avoid contact or collision, which could damage itself, the environment or humans working collaboratively. Soft arms theoretically need not abide by this restriction; soft robots should be able to collide with or even push past obstacles that cannot be avoided or are inconvenient to avoid. Though soft robotics research is often motivated by their inherent safety in contact and collision,
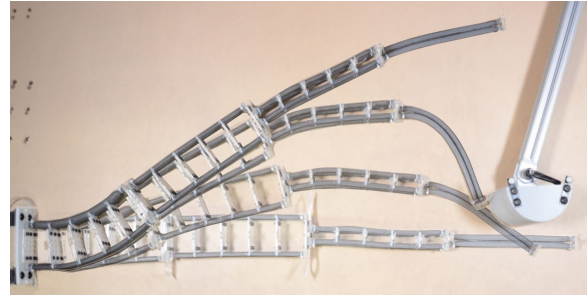

Fig. 1: Four segment arm successfully navigating past an obstacle through collision. The nominal width of each segment from the proximal to distal end is 49 mm, 42 mm, 7 mm, and 0 mm. Shading indicates temporal progression of arm, with darker shades representing later states.

there are no established guidelines on designing soft arms to successfully navigate past obstacles through collision.

When an arm interacts with the environment, it deforms, and the force causing that deformation must generally come from the arm. Successful environmental interactions depend on the arm's flexibility – its range of motion and its passive resistance to bending – and the arm's output force. Pushing past obstacles is a subset of environmental interactions that could expand a soft arm's workspace or create a simpler motion path, but to accomplish this the arm must be designed to succeed in these collisions. This paper examines how the design of soft arms affects their ability to navigate past obstacles in a collision-allowed analog to the obstacle-avoidance problem. This initial study considers planar arms pushing past a semi-circular obstacle at known distances from the arm's root (Figure 1).

Despite the inherent safety of soft arms in contact, there is little work on understanding the forces involved, implications of operation or development of planning techniques that can take advantage of collision. Soft grasping experiences notionally similar challenges, as the robot must conform to the object to grasp robustly [1]. However, soft grasping has no need to consider the further problem of navigating past an obstacle while in collision. Several soft arms have been used for whole arm grasping but again have not considered the further problem of collision-allowed motion [3], [4], [5]. One study examined the collision force between soft robots and obstacles to determine whether interactions with humans and soft robots are safe, but the study did not examine the success of the collision [6].

[1]Abigail Rafter is with the Department of Mechanical Engineering, Carnegie Mellon University (email: arafter@andrew.cmu.edu)

[2]Geoffrey A. Hollinger, Yiğit Mengüç and Gina Olson are with Collaborative Robotics and Intelligent Systems Institute at Oregon State University (email: geoff.hollinger@oregonstate.edu, yigit.menguc@oregonstate.edu, olsongi@oregonstate.edu).

[3]Yiğit Mengüç is also a Research Scientist at Facebook Reality Labs.

While previously studied soft robots are able to interact with their environments to move through tight or cluttered spaces, they do not do so by pushing past obstacles through collision. The STIFF-FLOP manipulator is proposed to maneuver through human bodies during invasive surgery by deforming itself to match its surroundings, but avoids contact [7]. Tube-climbing soft robots vary their diameter to brace against a cylindrical environment in order to climb or move forward [8]. Though these tube-climbing can push obstacles up to 10 times their weight out of the way, they do not squeeze into spaces smaller than their nominal body size. Quadrupedal walker robots use a wave-like activation pattern of their flexible body to crawl under obstacles without truly colliding, rather than taking advantage of their inherent softness to squeeze under [9]. Growing robots tackle navigating through environments by growing and reflecting off obstacles but not by pushing past them [10]. Other soft robots interact with obstacles by using sensors and controllers to map and detect the obstacles, but do not collide with them [11]. While these soft robots interact with their environments for navigation, the flexibility and durability of soft robots can be further exploited to allow for collision in order to take simpler paths when navigating through environments.

Current planners for soft arms use path planning algorithms for traditional hard robots and allow minimal to no interaction between the arms and obstacles, despite soft robots' inherent safety when interacting with their environments [3], [12]. Prior work has shown that the presence of obstacles, combined with the limited range of motion of soft arms, severely limits the accessible arm's workspace and thus the number of potentially successful paths [13]. However, path planning algorithms that allow for collision when they predict an arm can successfully push past the obstacle will expand the solution space and possibly uncover solutions to more challenging problems.

This paper addresses two aspects of operating soft arms in collision: first, it examines how varying the number of segments and taper ratios of planar soft arms affects their ability to navigate past obstacles and, second, it develops empirical models that may be used in a path planner to determine if an arm can successfully navigate past an obstacle through collision. Fourteen soft arms with different tapers and number of segments were tested to determine how these variables affect soft arms' ability to push past obstacles in a specified location. Ability was quantified by a binary metric for success and by measuring the actuator pressure required in successful cases. The contributions of this work are:

1) Experimental results of collisions between obstacles and soft robot arms with various designs.
2) Design guidance for planar soft arms that are intended to be used in collision.
3) An empirical model for individual soft arms to be used in conjunction with path planning algorithms to provide a go no-go decision.

Section II describes the arm designs tested and experimental methods. Fourteen planar arm designs with varying tapers and number of segments were tested. The segments are modular to allow the arm design to be varied efficiently. The effects of the selected arm design variables on the soft arms' ability to push past obstacles in given locations were analyzed for single and multiple segment actuation (Section III). An empirical model for obstacle nagivation success was developed for arms with constant taper ratios (Section III-C). The paper concludes with discussion on the trade-off between flexibility and force that must be considered when designing soft arms for collision (Section IV).

II. MATERIALS AND METHODS

Planar arms were tested in a representative but simplified collision case. The soft arms began next to a semi-circular obstacle that was centered at a known distance along the arm. When actuated by pressurization, the arm collided with the obstacle. Actuator pressure was increased until the arm pushed past the obstacle or reached the maximum allowed pressure. This case is closely representative of navigating past a too-close object in the environment or through a small gap in a wall.

Fourteen variants of the same planar arm design were tested. Variants were constructed by connecting modular planar arm segments of the same length and different widths together to form soft arms with different lengths and tapers. This section describes the modular arm design of a single planar segment, lists the variants tested and presents the experimental methods used for the collision tests.

A. Arm Design

Each arm segment consisted of McKibben actuators connected together. McKibben actuators contract when pressurized, which causes the segment to bend. McKibben actuators were chosen because they produce more force compared to extending actuators [14]. Prior work developed a robust manufacturing procedure for McKibben actuators and a modular key-and-slot arm architecture that was used in this work [15]. The design of the plates and caps were modified such that any two segments can be attached together. The plates were expanded to attach four actuators, with two on each side, and to include additional mounting to connect segments (Figure 3(a)). The caps were modified to have a flat top, a key out the side to attach to the plates and a barbed fitting on one end (Figure 3(b)).

Eight segments were built with widths ranging from 0 mm to 49 mm, in increments of 7 mm, where the segment widths are defined as the plate widths. The true width was 14 mm wider, due to the size of the actuators. Each segment was 210 mm long. Seven segments had four actuators each (Figure 2(c)), while the smallest segment, nominally 0 mm, had two (Figure 2(d)). The 0 mm had only end plates and the two actuators were tied together with thread in places. Plates were omitted due to the small size, but using thread also increased the segment's passive flexibility over what might be expected from narrowing it. The 0 mm segment was only used as the most distal segment in all arm variants.
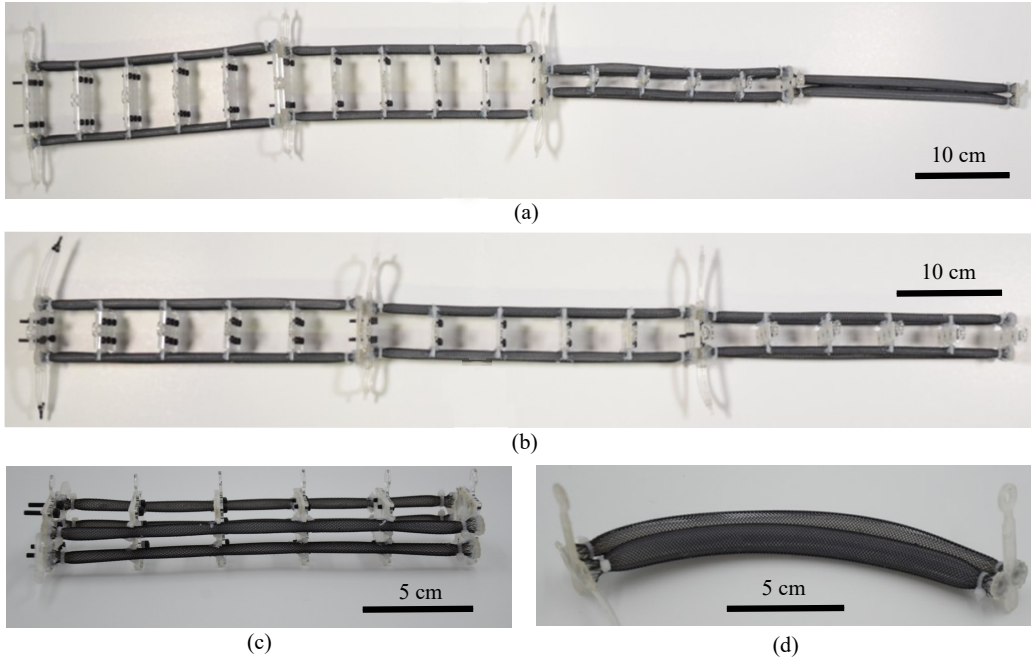
Fig. 2: Visual guide to arm design. (a) gives an example of a four segment arm with a non-constant taper. (b) gives an example of a three segment arm with a constant taper. (c) show the side view of a single segment with four actuators. (d) shows the two-actuator segment that was used as the distal segment in most of the arms tested.
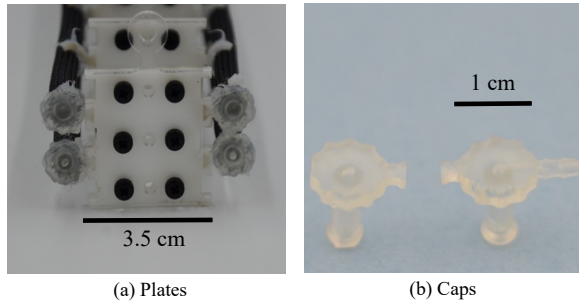

Fig. 3: Plates and caps used as part of the modular arm design. (a) The plates used to connect the actuators on each side of a segment together. (b) The caps, which were printed using a FormLabs Form 2, that close the actuator ends, attach to the plates and provide an air inlet.

The arm taper is defined by how much the widths of the segments decrease from the proximal (root, base) to distal (tip) end. Arms of 2, 3, and 4 segments of constant and non-constant tapers were tested (Figure 2(a) and (b)). Arms consisting of a single segment were not tested because this paper examines the ability of active proximal segments to push passive distal segments past obstacles, and an arm with only one segment cannot have both active and passive segments. A 7 mm constant taper decreases nominal widths by 7 mm in each subsequent segment, e.g., 14 mm, followed by 7 mm and ending with 0 mm. The arms tested are denoted by the widths of their segments, listed from proximal to distal. Examples of this notation can be seen in Figure 4.

TABLE I: List of arms tested.

Two Segments	Three Segments	Four Segments
7-0 mm	14-7-0 mm	21-14-7-0 mm
28-0 mm	28-14-0 mm	42-28-14-0 mm
49-0 mm	49-7-0 mm	49-42-7-0 mm
14-7 mm	21-14-7 mm	
49-7 mm	42-21-0 mm	
	49-7-0 mm	

The tested variants are listed in Table I.

B. Experimental Setup

A testbed was constructed that contains the semi-circular obstacle and the planar arm being tested (Figure 5). The obstacle was attached to a two-link arm made from 80/20 extrusions, and the two-link arm was connected to a base 80/20 bar (Figure 5 at B) anchored to the test bed. Locking pivot joints were used to connect the base, arm links and obstacle, which allowed the obstacle to be rigidly positioned anywhere in the testbed. The soft arms were anchored to the testbed on the opposite side (Figure 5 at A). A dry lubricant was applied to the testbed prior to testing in order to reduce friction between the bed and the soft arms.

The soft arms were manually pressurized via syringe connected to a visual pressure gauge, and a second pressure sensor (Honeywell TruStability HSCDRRN30PG) was read through an Arduino and used to record actuator pressure during tests. An OptiTrack Motion Capture system was used to track the motion of the arm using retroreflective markers that were connected to each plate through the hole at the top
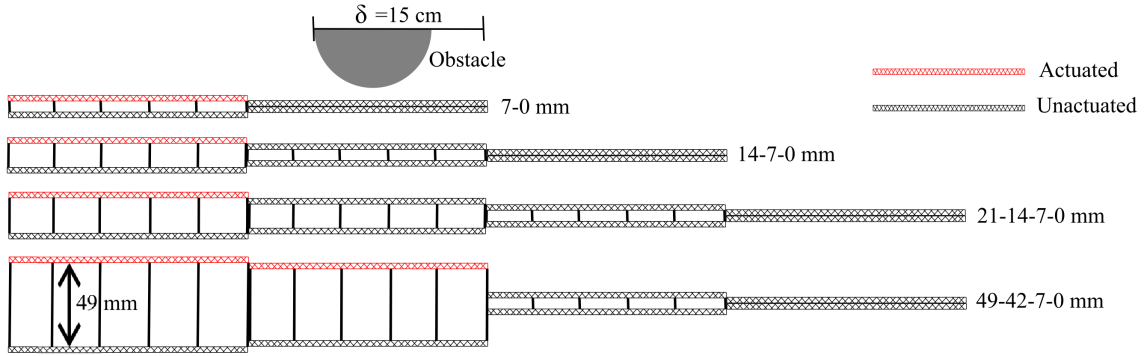
Fig. 4: Naming convention for the tested arms and definition of δ. The width of each segment from proximal to distal end is represented in the corresponding number in the name. The hatched lines indicate the McKibben actuators and the vertical black lines indicate the plates. The top three arms are the 2, 3, and 4 segment 7 mm constant taper arms with the proximal segment actuated. The bottom arm shows a non-constant taper ratio arm undergoing multiple segment actuation. The obstacle location δ is measured from the distal tip of the arm to the far end of the obstacle.

(Figure 3(a)). The total number of markers varied by arm, but equaled the number of plates in the arm. Markers were also mounted to the edge of the obstacle.

C. Testing Procedure

The obstacle began centered on the distal tip of the arm being tested. The amount of interference is given by δ and is defined as the parallel distance from the distal tip of the arm to the edge of the obstacle closest to the arm's root (Figure 4. The initial obstacle position is equivalent to $\delta = 5$ cm. Obstacle locations were limited to a line parallel to the arm's initial axis. This method of varying the location of the obstacle in only one dimension was chosen because it was easily quantifiable and comparable between arms.

Three trials were run for each obstacle location. A single trial consisted of pressurizing one or multiple segments until the arm passed the obstacle or reached the maximum pressure. Actuator pressure and marker position were monitored and recorded continuously during each trial. If the arm was
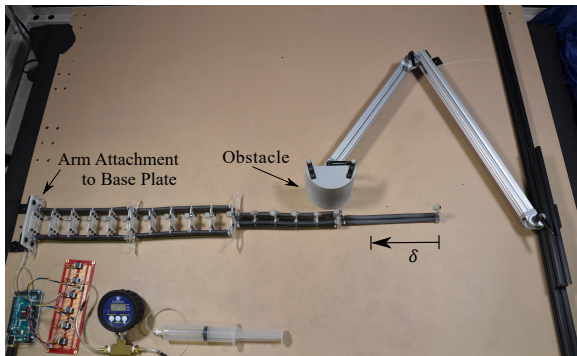

Fig. 5: Experiment testbed. The obstacle was mounted to a rigid, lockable two link arm. Two pressures gauges were used to monitor and record actuator pressure. δ represents the obstacle interference distance.

able to pass the obstacle at a given location δ was increased by 2 cm, moving the obstacle closer to the arm's root. If the arm failed to pass the obstacle trials were taken at 0.5 cm intervals between the failed and last successful location.

Either 1, 2, or 3 segments were actuated in the same direction during a trial. Segments were actuated by pressurizing one actuator to induce a bend. Regardless of the number of actuated segments, all actuated segments were connected to the same input to achieve the same pressure in each. The most distal segment was never actuated. Although actuator pressure was recorded throughout each trial, the pressure required to pass an obstacle was considered to be the pressure when the arm was on verge of passing the obstacle during successful tests. This point was determined by identifying the minimum distance between the retroreflective markers on the tip of the soft arm and the edge of the obstacle. The trials were only considered successful if the arm completely passed the obstacle and was no longer in contact.

III. RESULTS

This section presents the single- and multiple-segment actuation test results. All plots show the average result, with the span of results represented by error bars. Generally, the repeated tests varied little, showing that the system is repeatable and deterministic even when manually pressurized by syringe. All plots show only successful trials. Obstacle distances beyond those shown were tested and the final plotted point may be considered the maximum allowable δ.

A. Single Segment Actuation

The results of actuating only the proximal segment for all arm variants are shown in Figure 6. Results are grouped by the number of segments and arms with things groups were the same length. Segment widths of each variant are identified by the legend labels. The interference distance δ is measured from the arm's distal end to the edge of the obstacle nearest the arm's root; measurements were

not taken for $\delta < 5$ cm. Arms that had larger spans of successful obstacle locations are considered to perform better and generally correlated to lower actuator pressures at any given location. The results of the single segment actuation tests demonstrate the importance of three aspects of the arm's design: passive stiffness (or flexibility) of the distal segment, force produced by the proximal segment and stroke of the proximal segment. Arm length and the compliance of intermediate segments affected performance more subtly.

The worst performing arms had a 7 mm distal segment instead of 0 mm. The 7 mm segment was much stiffer than the 0 mm segment due to, first, a higher geometric stiffness from the larger width and, second, the addition of support plates. Even though the width increase was small, the increase in stiffness from the 0 mm to 7 mm segment was nearly impossible for any arm design to overcome (Figure 6(a) and (b)). This severe loss of performance demonstrates the need for narrow, highly flexible distal segments. If a
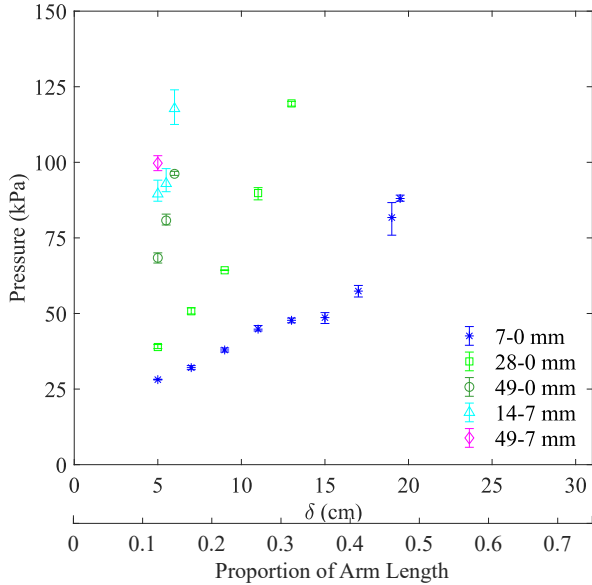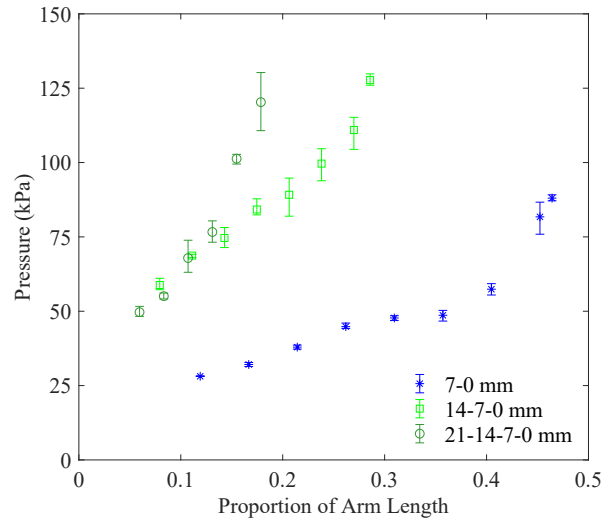

(a) Two Segment Arms
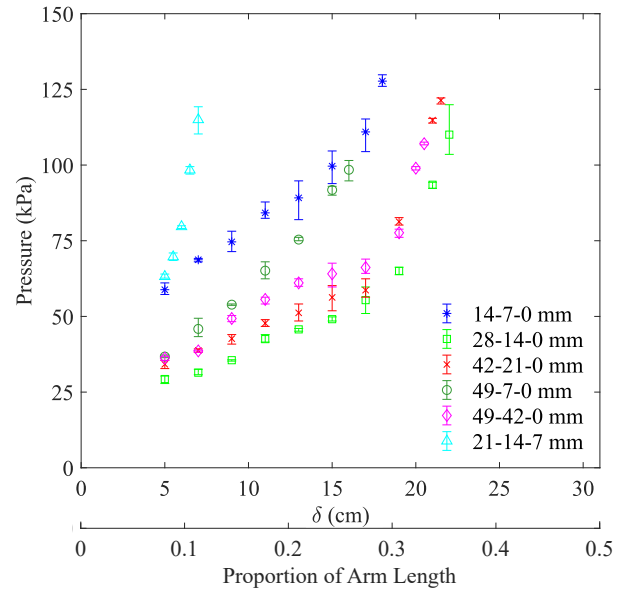
(b) Three Segment Arms
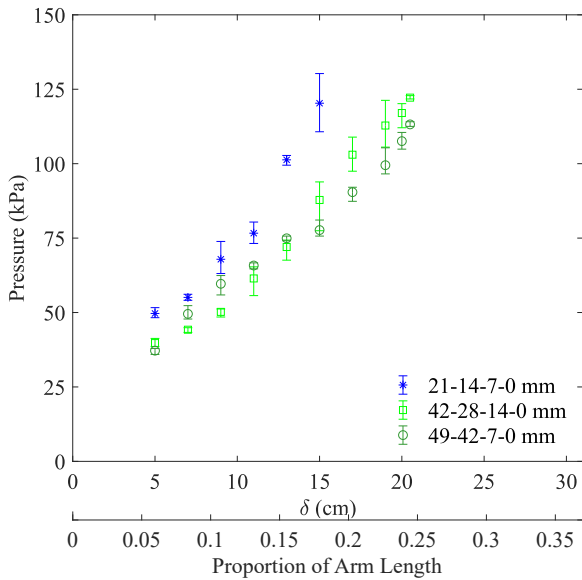
(c) Four Segment Arms

(d) 7 mm Constant Taper Ratio Arms

Fig. 6: Single segment actuation. The minimum pressure required for an arm to successfully push past an obstacle in a given location measured from the distal end of each arm (δ). (a), (b), and (c) give the results for two, three, and four segment arms, respectively. (d) compares the results for the two, three, and four segment 7 mm constant taper arms with respect to the location of the obstacle as a proportion of the arm length.

wider distal segment is required, the proximal segment must produce a larger force to overcome the stiffness.

Segment force increases with segment width and actuator pressure (for a given actuator), which can be used to overcome passive stiffness. The 14-7-0 mm and 28-14-0 mm arms have narrower widths than the other three segment arms and must operate at higher pressures in order to produce the required force, as shown in Figure 6b. Similarly, the 21-14-7-0 mm arm must operate at higher pressure than the other four segment arms (Figure 6c). When the force required to move past an obstacle increases beyond what the narrower segments can produce at their maximum pressure, arms with narrower segments bind against the obstacle.

However, increasing segment force by increasing width has the counter effect of decreasing segment stroke. A planar arm segment's stroke, or range of curvature and motion, is inversely proportional to the segment's width [13] and can be assumed to be further reduced by load on the arm. The effect of width and stroke on the shape of the arm in collision is visible in Figure 7 and a minimum stroke is required to pull the arm tip fully past an obstacle. The 7-0 mm arm had the narrowest proximal segment of the

two segment arms and therefore the largest stroke, and it performed the best. The 49-0 mm arm performed the worst (excepting the arms with a 7 mm distal segment) even though it nominally had the highest force (Figure 6a). An ideal balance between force and stroke is shown in Figure 6(b) for the three segment arms. Increasing segment widths from 14-7-0 mm to 28-14-0 mm improves performance, while further increasing segment widths degrades performance. This optimal proximal segment width shifts as the number of segment increases, and the optimal width for four segments is between 42 mm and 49 mm (Figure 6(c)).

Arm length affects the required stroke and the resisting friction force for planar arms. For the same angular stroke, the arc length swept out by the distal segment is longer for longer arms, but the total friction force on the arm is also higher and has a longer lever. The results suggest that the increased friction quickly dominates arm behavior. Figure 6d shows the pressure required to move past an obstacle with respect to obstacle location as a proportion of arm length for the two, three and four segment 7 mm taper arms. Though the arms have the same relative dimensions, the 7 mm taper design is proportionally less successful the longer the arm
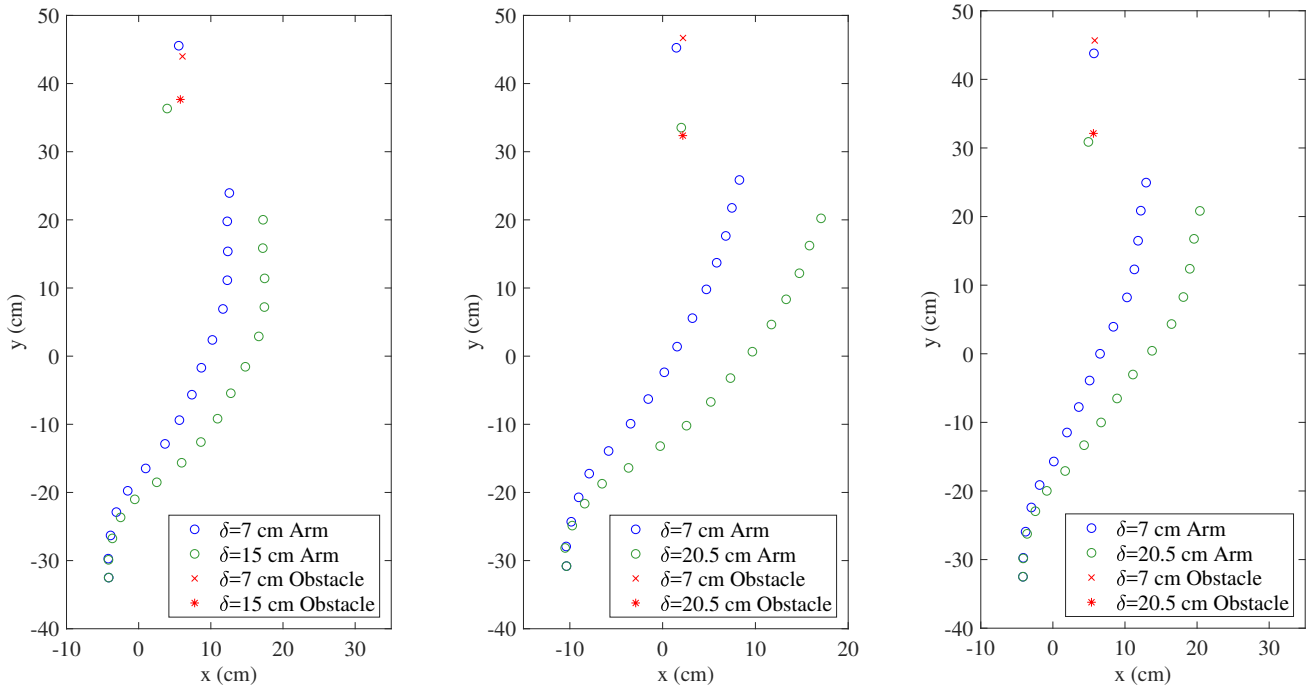
(a) 21-14-7-0 mm
$\delta = 7$ cm : Pressure= 30 kPa
$\delta = 15$ cm : Pressure= 120 kPa

(b) 42-28-14-0 mm
$\delta = 7$ cm : Pressure= 27 kPa
$\delta = 20.5$ cm : Pressure= 123 kPa

(c) 49-42-7-0 mm
$\delta = 7$ cm : Pressure= 23 kPa
$\delta = 20.5$ cm : Pressure= 112 kPa

Fig. 7: Plots of the locations of the reflective beads attached to three arms and obstacles just before each arm pushes past the obstacle. (a), (b), and (c) each contain two instances of a given arm for different obstacle locations: $\delta = 2$ cm and the maximum δ for each arm. Retroreflective markers could only be attached to the ends of the distal segment because there were only plates on the end, so only these points are plotted for the distal segment. The red markers signifies the lowest edge of the obstacle and the last point of collision. (x,y) represent OptiTrack coordinates.

gets. The increased friction requires higher forces from the proximal segment, which favors wider designs for longer arms. Four segment arms performed best with proximal segment widths of 42 mm and 49 mm (Figure 6(c)).

The last effect of note is the compliance of intermediate segments. Segments with a higher passive stiffness perform more effectively than segments with lower passive stiffness. This trend can be seen in the superior performance of the 49-42-0 mm over 49-7-0 mm arm (Figure 6(b)) and in the differing shapes of the 42-28-14-0 mm and 49-42-7-0 mm arms (Figure 7(b) and (c)). The results suggest that wider, stiffer intermediate segments deform less and concentrate applied force and deformation in the distal segment.
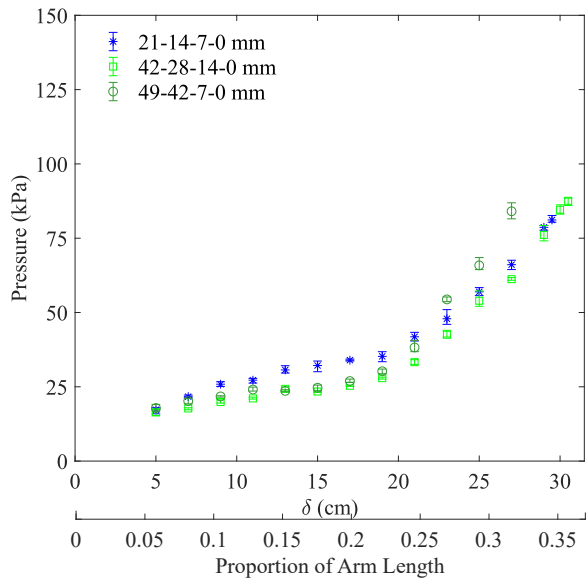
No single design variable predicts an arm's success in collision because each is interconnected to a metric of performance. Stroke increases as segment width decreases
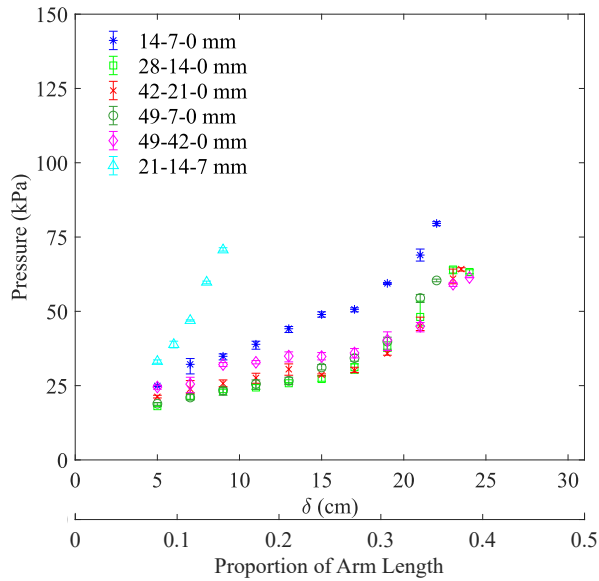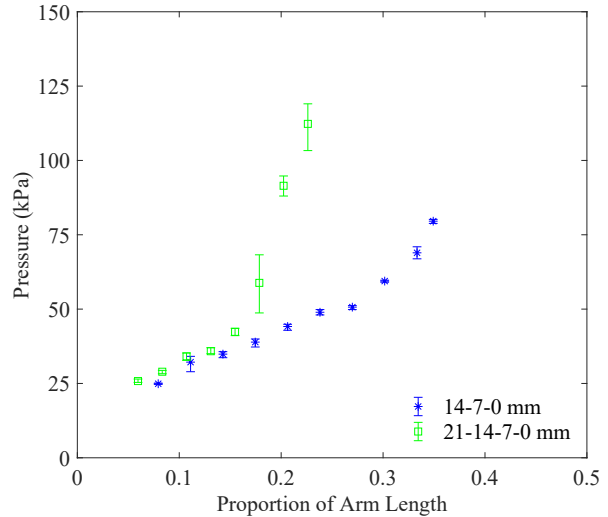

(a) Three Segment Arms with Two Segment Actuation
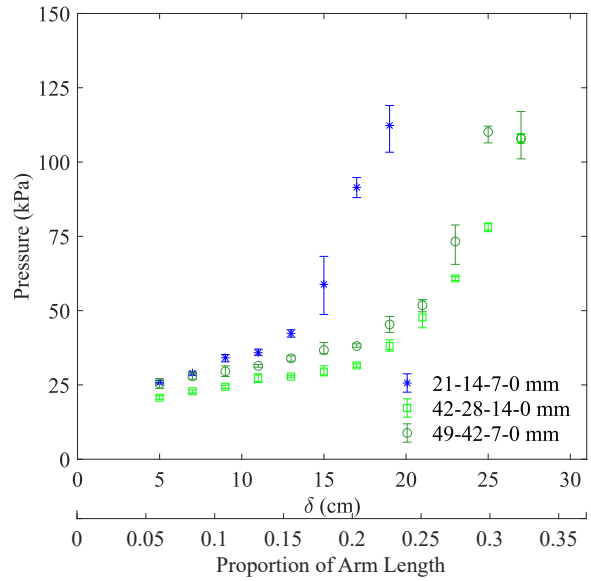
(b) Four Segment Arms with Two Segment Actuation

(c) Four Segment Arms with Three Segment Actuation

(d) 7 mm Constant Taper Ratio Arms with Two Segment Actuation

Fig. 8: Multiple segment actuation. The minimum pressure required for an arm to successfully push past an obstacle in a given location measured from the distal end of each arm (δ). (a) gives the results for three segment arms with the distal two segments being actuated. (b) and (c) give the results for four segment arms with the distal two and three segments being actuated, respectively. (d) compares the results for the three and four segment 7 mm constant taper arms with two actuated segments with respect to δ as a proportion of the arm length measured.

and arm length increases. However, arm force decreases as segment width decreases, and the friction force against the arm increases with length. Passive stiffness is also driven by width and ideally high when transferring force and low when deforming. Arm designs that are successful in collision effectively balance flexibility and force. Each arm length demonstrates a different ideal balance, which manifests as a shifting optimum taper.

B. Multiple Segment Actuation

The arm variants were also tested with multiple actuated segments, though segments were always actuated in the same direction (Figure 8). The results show similar trends to single segment actuation (e.g., 7 mm distal segments perform poorly, as do long and narrow arms), but the performance span is reduced. The greater the number of actuated segments as a fraction of the total number of segments, the more similar the results, though longer arms with 7 mm distal tips were not tested. When three of four segments are actuated, the performance becomes nearly identical (Figure 8(c)). This performance improvement may occur as a result of higher arm force, or it may be caused by a changing direction of contact from multiple actuated segments. However, the improvement suggests a potential advantage to a higher number of segments than are normally needed for reaching.

C. Model

The results from this study can be used as part of a motion planner to predict whether a given arm will be able to successfully navigate past a given obstacle through collision. Parabolic curves were fit to each of the constant taper arms to express the relationship between the location of an obstacle (δ) and the pressure required for a given arm to move past the obstacle (Table II). Any pressure higher than the pressure from the fit curve for a given arm would successfully navigate the arm past an obstacle. All of the R^2 values are above 0.920 with the highest being 0.994.

$$\text{Pressure (kPa)} = a\delta^2 + b\delta + c \qquad (1)$$

TABLE II: Experimental fits for constant taper arms with single segment actuation. Constants a, b, and c are from Eq. 1. Max δ is the largest successful interference distance.

	a	b	c	R^2	Max δ (cm), % Length
7-0 mm	0.268	-3.01	39.9	0.941	19.5, 46.4%
14-7-0 mm	0.194	0.231	55.4	0.978	18.0, 28.6%
28-14-7-0 mm	0.516	-3.16	52.5	0.993	15.0, 17.9%
28-14-0 mm	0.436	-7.04	65.2	0.950	22.0, 34.9%
42-28-14-0 mm	0.136	2.09	23.5	0.994	20.5, 24.4%
42-21-0 mm	0.207	-1.47	41.2	0.922	21.5, 34.1%

IV. CONCLUSION

Soft robot arms are motivated by operating in collision, but they are rarely studied in collision. This paper has sought to identify design guidelines for soft arms operated in collision and has found that flexibility and force must be balanced. Wider proximal segments produce more force to overcome tip stiffness and arm friction, but have a smaller stroke which limits tip displacement. Widening the proximal segment is only useful to a point and then begins to limit obstacles locations that the arm can navigate past. Most significantly, this work has identified that the ideal taper for collisions shifts as the arm lengthens. The next step in this work is to create a model that can determine the pressure required for a given arm design to navigate past a broader variety of obstacles and locations. This model could help inform collision-allowed motion planning and design.

REFERENCES

[1] J. Amend, E. Brown, N. Rodenberg, H. Jaeger, and H. Lipson, "A positive pressure universal gripper based on the jamming of granular material," *IEEE Trans. on Robotics*, vol. 28, no. 2, pp. 341–350, 2012.

[2] E. Hawkes, L. Blumenschein, J. Greer, and A. Okamura, "A soft robot that navigates its environment through growth," *Science Robotics*, vol. 2, 2017.

[3] A. Marchese, R. Katzschmann, and D. Rus, "Whole arm planning for a soft and highly compliant 2d robotic manipulator," *Proc. IEEE/RSJ Int. Conference on Intelligent Robots and Systems (IROS)*, 2014.

[4] I. Walker, D. Dawson, T. Flash, F. Grasso, R. Hanlon, B. Hochner, W. Kier, C. Pagano, C. Rahn, and Q. Zhang, "Continuum robot arms inspired by cephalopods," *Proceedings SPIE Conference on Unmanned Ground Vehicle Technology VII*, pp. 303–314, 2005.

[5] P. H. Nguyen, C. Sparks, S. G. Nuthi, N. M. Vale, and P. Polygerinos, "Soft poly-limbs: Toward a new paradigm of mobile manipulation for daily living tasks," *Soft Robotics*, vol. 6, no. 1, pp. 38–53, 2019.

[6] J. Kim, A. Alspach, and K. Yamane, "3d printed soft skin for safe human-robot interaction," *Proc. IEEE/RSJ Int. Conference on Intelligent Robots and Systems (IROS)*, pp. 2419–2425, 2015.

[7] M. Cianchetti, T. Ranzani, G. Gerboni, I. D. Falco, C. Laschi, and A. Menciassi, "Stiff-flop surgical manipulator: mechanical design and experimental characterization of the single module," *Proc. IEEE/RSJ Int. Conference on Intelligent Robots and Systems (IROS)*, 2013.

[8] M. Verma, A. Ainla, D. Yang, D. Harburg, and G. Whitesides, "A soft tube-climbing robot," *Soft Robotics*, vol. 5, no. 2, pp. 133–138, 2018.

[9] R. Shepherd, F. Ilievski, W. Choi, S. A. Morin, A. A. Stokes, A. D. Mazzeo, X. Chen, M. Wang, and G. M. Whitesides, "Multigait soft robot," *Proceedings of the National Academy of Sciences*, vol. 108, no. 51, pp. 20400–20403, 2011.

[10] J. Greer, L. Blumenschein, R. Alterovitz, E. Hawkes, and A. Okamura, "Robust navigation of a soft growing robot by exploiting contact with the environment," *arXiv:1908.08645*, 2019.

[11] K. C. Galloway, Y. Chen, E. Templeton, B. Rife, I. Godage, and E. Barth, "Fiber optic shape sensing for soft robotics," *Soft Robotics*, vol. 6, no. 5, 2019.

[12] I. S. Godage, D. T. Branson, E. Guglielmino, and D. G. Caldwell, "Path planning for multisection continuum arms," *Proc. IEEE Int. Conf. on Mechatronics and Automation*, pp. 1208–1213, 2012.

[13] G. Olson, S. Chow, A. Nicolai, C. Branyan, G. Hollinger, and Y. Mengüç, "A generalizable equilibrium model for bending soft arms with longitudinal actuators," *The International Journal of Robotics Research*, vol. Advance online, 2019.

[14] T. E. Pillsbury, Q. Guan, and N. M. Wereley, "Comparison of contractile and extensile pneumatic artificial muscles," *Proc. IEEE Int. Conference on Advanced Intelligent Mechatronics (AIM)*, 2016.

[15] G. Olson, B. Woronowicz, and Y. Mengüç, "Characterization of a class of soft bending arms," *Proc. IEEE Int. Conf. on Soft Robotics (RoboSoft) Livorno, Italy*, 2018.